ELSEVIER

Nuclear Physics A 594 (1995) 175–202

NUCLEAR PHYSICS A

Superdeformed triaxial bands in ^{163,165}Lu

H. Schnack-Petersen [a], R. Bengtsson [b], R.A. Bark [a,c], P. Bosetti [a,1], A. Brockstedt [c], H. Carlsson [c], L.P. Ekström [c], G.B. Hagemann [a], B. Herskind [a], F. Ingebretsen [d], H.J. Jensen [a], S. Leoni [a], A. Nordlund [c], H. Ryde [c], P.O. Tjøm [d], C.X. Yang [c,2]

[a] *The Niels Bohr Institute, Tandem Accelerator Laboratory, DK-4000 Roskilde, Denmark*
[b] *Department of Mathematical Physics, University of Lund, Box 118, S-221 Lund, Sweden*
[c] *Department of Physics, University of Lund, S-223 62 Lund, Sweden*
[d] *Department of Physics, University of Oslo, N-0316 Oslo, Norway*

Received 13 July 1995

Abstract

An experimental investigation of the nucleus ^{165}Lu, using the reactions ^{138}Ba(^{31}P,4n)^{165}Lu and ^{150}Sm(^{19}F,4n)^{165}Lu at beam energies of E = 155 and 95 MeV, respectively, has been performed. Among other additions to the existing level scheme, a new band, with transition energies almost identical to a strongly deformed ($\beta_2 \sim 0.42$) $\pi i_{13/2}[660\ 1/2^+]$ band recently discovered in ^{163}Lu has been established. A theoretical analysis of the structure of the two Lu isotopes, ^{165}Lu and ^{163}Lu is carried out by detailed calculations of total potential energy surfaces for specific configurations. By a diabatic treatment of crossings specific proton configurations as $\pi i_{13/2}[660\ 1/2^+]$ are identified throughout the deformation space and as a function of spin. It is found as a general feature that well deformed local minima of considerable nonaxial symmetry coexist with a normal deformed global minimum. The depth of these local minima depend on configuration. The structure of the different global and local minima found in these surfaces are analysed and discussed in terms of occupation of available basis configurations and their orientation relative to the rotation axis. The strongly deformed minima are found to belong to a group of superdeformed triaxial structures, expected to appear at low energies for certain favourable combinations of proton and neutron numbers.

Keywords: Nuclear reactions ^{138}Ba(^{31}P,4n)^{165}Lu and ^{150}Sm(^{19}F,4n)^{165}Lu, E = 155 and 95 MeV; measured E_γ, γ-γ coin, I_γ. ^{165}Lu deduced levels, $i_{13/2}[660\ 1/2^+]$ rotational band-structure. Enriched target, array of Compton suppressed Ge-detectors. Calculation of superdeformed highly triaxial local minima in configuration separated total energy surfaces (TES).

SSDI 0375-9474(95)00363-0

1. Introduction

Rotational bands built on the proton $i_{13/2}[660\ 1/2^+]$ intruder orbital are known in the heavier rare earths odd-Z nuclei. This orbital is predicted [1] to polarize the nucleus in the prolate direction. A moderately increased deformation for this band has indeed been found in ^{179}Ir [2]. A theoretical investigation of the shape evolution of these intruder bands can be found in Ref. [3], which also contains references for experimental $i_{13/2}[660\ 1/2^+]$ bands in Re and Ir isotopes. With decreasing Z the $i_{13/2}[660\ 1/2^+]$ orbital moves further away from the Fermi surface, and is therefore more difficult to establish experimentally, unless a larger increase in deformation is encountered, which brings it closer to the Fermi level.

Recently a strongly deformed rotational band has been discovered [4,5] in ^{163}Lu with $\beta_2 \sim 0.42$. Based on the large deformation, this band was interpreted as corresponding to the $\pi i_{13/2}[660\ 1/2^+]$ configuration [4,5]. A local minimum with large deformation was found in total routhian surface (TRS) calculations for ^{163}Lu in the lowest surface with $(\pi, \alpha) = (+, +1/2)$. The calculated deformation is in qualitative agreement with the measured quadrupole moments [5,6].

2. Measurements in ^{165}Lu

The nucleus ^{165}Lu has been studied by employing the two reactions, ^{138}Ba(^{31}P,4n)^{165}Lu and ^{150}Sm(^{19}F,4n)^{165}Lu, at bombarding energies of 155 and 95 MeV, respectively from the NBI heavy ion tandem plus booster accelerator. Gamma rays were measured in the NORDBALL detector array [7,8] with 20 Compton suppressed Ge detectors and an inner ball of 60 BaF_2 scintillators, providing the γ-ray multiplicity and sum-energy used for selecting the different xn channels. The target for the ^{31}P induced experiment consisted of 300 μg/cm^2 ^{138}Ba, enriched to 99.8%, on a thin (~ 0.5 mg/cm^2) supporting Au foil facing the beam. For the ^{19}F induced reaction two stacked self-supporting ^{150}Sm foils of 680 μg/cm^2 enriched to 95.5% were used.

To produce $\gamma\gamma$-matrices, energy dependent time gates were used to reduce background, in particular from neutron induced γ-radiation. Gating conditions for sum-energy and fold were chosen to enhance the 4n reaction. The fold gates were 11 and 7 for the ^{31}P and ^{19}F induced reactions respectively, reflecting a difference in the fold distribution due to a difference in the maximum angular momentum input of 58 $\hbar$ and 35 $\hbar$. A total of $\sim$ 115 and $\sim$ 280 million "clean" 4n events were obtained in the two reactions after applying the time and fold gates.

[1] Permanent address: Department of Physics, University of Milano, Italy.
[2] Permanent address: Institute of Atomic Energy, Beijing, P.R. China.

3. Experimental analysis and results

The $\gamma\gamma$-matrices from both experiments have been analysed with the Radware analysis program package (ESCL8R) [9].

Most of the previously known [10,11] rotational bands in this nucleus could be considerably extended. A partial level scheme showing the positive parity bands, pertinent for the present investigation which focuses on the [660 1/2$^+$] band, is shown in Fig. 1. A list of energies and intensities of the transitions associated with these positive parity bands is presented in Table 1. The two known negative parity bands, [541 1/2$^-$] and [514 9/2$^-$], as well as several new side bands are omitted in Fig. 1 and Table 1. Bands built on the normal positive parity configurations, [404 7/2$^+$], [411 1/2$^+$] and [402 5/2$^+$] are strongly mixed at certain spin values. The [404 7/2$^+$] band is the only one of the three bands, which is established to spins higher than 29/2 $\hbar$. It feeds into both the [402 5/2$^+$] and the [411 1/2$^+$] bands at I = 25/2 and 27/2 $\hbar$ respectively. Furthermore, the analysis of the [404 7/2$^+$] band is complicated by feeding from a new band. By rejecting the possibility of M2 transitions, and considering the mutual decay pattern, the new band can be determined to have positive parity and spin values as given in the level scheme. The new band is most likely of three-quasiparticle nature. It is evidently strongly mixed with the [404 7/2$^+$] band over a spin range of 5–6 $\hbar$, and carries most of the intensity in the positive parity sequences for $I \geqslant 39/2\hbar$. Accordingly, the [404 7/2$^+$] band could only be extended to 51/2 and 37/2 $\hbar$ for the negative and positive signatures, respectively.

The three-quasiparticle band has rather strong M1 interband transitions in competition with the in-band E2 transitions. The experimental values of $B(\mathrm{M1})/B(\mathrm{E2}) \sim 1.5\ \mu_N^2/e^2b^2$, increase to $\sim 2\mu_N^2/e^2b^2$ at a crossing occurring around $\hbar\omega_c = 0.31$ MeV. We interpret this band as corresponding to a quasiproton in the [514 9/2$^-$] configuration coupled to two quasineutrons, in the $i_{13/2}$[642 5/2$^+$] and the [523 5/2$^-$] configurations. These correspond to the A and E quasineutrons coupled to $(\pi, \alpha) = (-, 1)$. This configuration is known as the lowest negative parity band in neighbouring even–even nuclei, and in ^{166}Hf it comes close to the yrast line at $I \sim 28\ \hbar$. The crossing can be understood as caused by the BC quasineutrons crossing at approximately the expected frequency. This interpretation is consistent with the observed values of $B(\mathrm{M1})/B(\mathrm{E2})$.

In addition, a rotational band with transition energies identical (within 1–2 keV) to those in the strongly deformed band in ^{163}Lu was found. The fact that the yrast band in ^{163}Lu was not observed in the present experiments rules out the possibility that the new band belongs to ^{163}Lu. Indeed, connections to known band structures in ^{165}Lu have been found. Because of the similar transition energies we interpret this new band in ^{165}Lu as also associated with the [660 1/2$^+$] intruder configuration. In favour of this interpretation is the lack of signature partners in both ^{163}Lu and ^{165}Lu.

A spectrum corresponding to a sum of very narrow gates on transitions in this new [660 1/2$^+$] band is shown in the lower part of Fig. 2. It decays into the [411 1/2$^+$], [402 5/2$^+$], and the [404 7/2$^+$] bands. The decay pattern is difficult to trace due to the presence of mixing and all the connecting transitions have not been firmly estab-

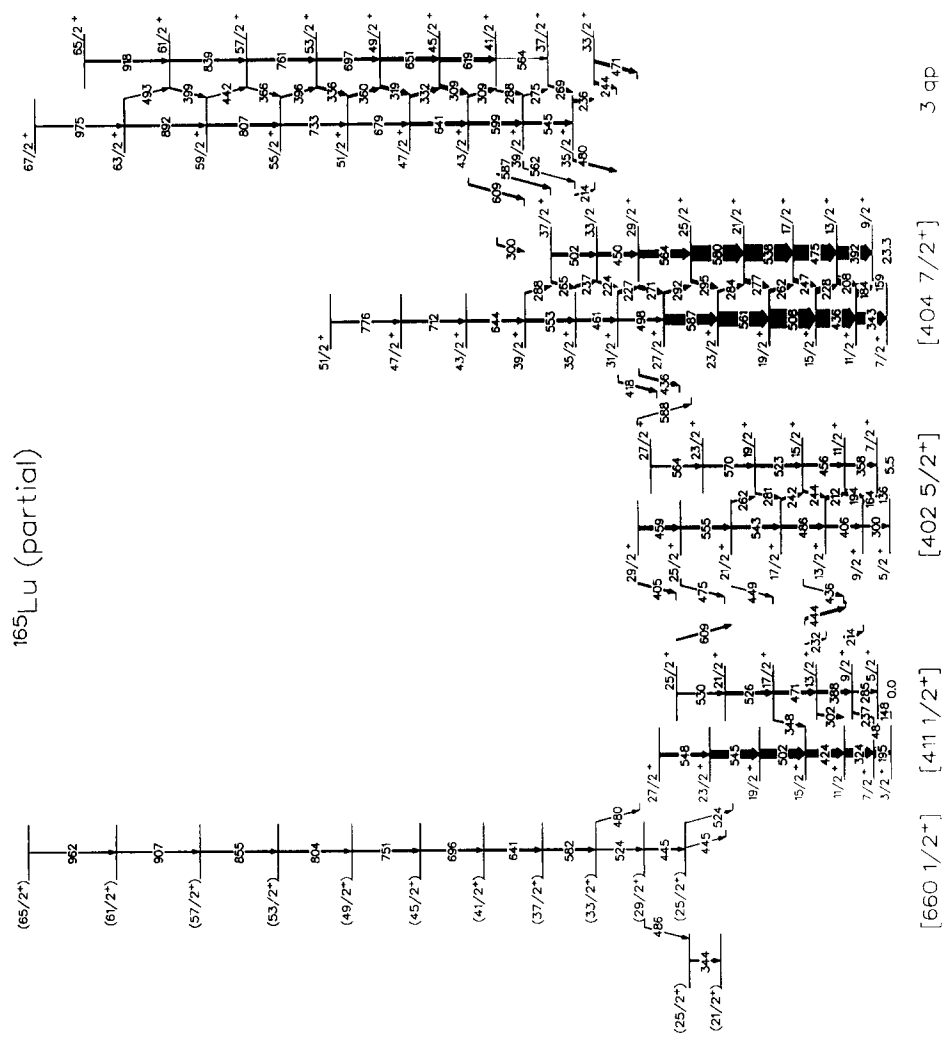

Fig. 1. Partial level scheme of the selected positive parity bands related to the $i_{13/2}$ [660 1/2$^+$] band.

Table 1
Energy (E_γ), relative intensity (I_γ,^{31}P and I_γ,^{19}F), initial and final state energies (E_i and E_f) and initial and final spin (J_i and J_f) for transitions in the positive parity bands in ^{165}Lu

E_γ	I_γ,^{31}P	I_γ,^{19}F	E_i	E_f	J_i	J_f
γ-rays from states in the [404 7/2$^+$] band						
159.18(11)	10.0(10)	10.0(10)	182.4(1)	23.3	9/2$^+$	7/2$^+$
184.27(11)	85.7(19)	124.3(22)	366.6(1)	182.4	11/2$^+$	9/2$^+$
207.59(12)	61.5(11)	92.4(13)	574.1(1)	366.6	13/2$^+$	11/2$^+$
214.14(26)	10.4(5)	16.2(5)	3417.3(4)	3201.1	35/2$^+$	33/2$^+$
224.33(16)	15.4(5)	21.6(5)	3180.4(4)	2956.8	33/2$^+$	31/2$^+$
226.52(14)	27.7(7)	41.0(8)	2956.8(3)	2730.3	31/2$^+$	29/2$^+$
228.18(14)	46.0(9)	67.0(10)	802.2(1)	574.1	15/2$^+$	13/2$^+$
237.23(14)	19.7(6)	24.7(6)	3417.3(4)	3180.4	35/2$^+$	33/2$^+$
246.69(13)	33.8(7)	48.8(7)	1048.8(2)	802.2	17/2$^+$	15/2$^+$
262.00(14)	28.3(7)	43.3(8)	1310.7(2)	1048.8	19/2$^+$	17/2$^+$
265.33(14)	20.1(6)	22.5(5)	3682.6(5)	3417.3	37/2$^+$	35/2$^+$
271.40(14)	36.1(7)	40.0(6)	2730.3(3)	2458.7	29/2$^+$	27/2$^+$
276.52(13)	38.5(7)	49.0(8)	1587.1(2)	1310.7	21/2$^+$	19/2$^+$
284.49(15)	17.6(7)	24.7(6)	1871.7(2)	1587.1	23/2$^+$	21/2$^+$
287.64(95)	14.9(7)	15.7(6)	3970.2(14)	3682.6	39/2$^+$	37/2$^+$
291.80(14)	24.2(6)	26.4(6)	2458.7(3)	2166.8	27/2$^+$	25/2$^+$
295.04(14)	28.6(6)	30.6(6)	2166.8(2)	1871.7	25/2$^+$	23/2$^+$
343.03(12)	120.9(31)	146.2(30)	366.6(1)	23.3	11/2$^+$	7/2$^+$
391.71(11)	142.6(24)	180.9(24)	574.1(1)	182.4	13/2$^+$	9/2$^+$
418.06(14)	20.1(4)	20.3(4)	2956.8(3)	2538.7	31/2$^+$	27/2$^+$
435.61(12)	183.0(25)	201.7(24)	802.2(1)	366.6	15/2$^+$	11/2$^-$
435.82(16)	20.8(8)	27.9(7)	2730.3(3)	2294.6	29/2$^+$	25/2$^-$
450.08(13)	43.6(9)	44.2(8)	3180.4(4)	2730.3	33/2$^+$	29/2$^-$
460.51(15)	32.7(10)	42.3(9)	3417.3(4)	2956.8	35/2$^+$	31/2$^-$
474.73(12)	163.6(20)	194.7(20)	1048.8(2)	574.1	17/2$^+$	13/2$^-$
498.27(18)	23.0(7)	28.4(6)	2956.8(3)	2458.7	31/2$^+$	27/2$^+$
502.04(16)	34.2(10)	36.7(9)	3682.6(5)	3180.4	37/2$^+$	33/2$^+$
508.41(12)	197.1(20)	242.4(20)	1310.7(2)	802.2	19/2$^+$	15/2$^+$
538.25(12)	174.9(18)	204.5(17)	1587.1(2)	1048.8	21/2$^+$	17/2$^+$
552.90(95)	36.5(10)	33.5(9)	3970.2(14)	3417.3	39/2$^+$	35/2$^+$
561.03(13)	151.6(20)	161.8(18)	1871.7(2)	1310.7	23/2$^+$	19/2$^+$
563.56(14)	84.0(16)	90.6(15)	2730.3(3)	2166.8	29/2$^+$	25/2$^+$
579.74(12)	165.0(18)	31.6(9)	2166.8(2)	1587.1	25/2$^+$	21/2$^+$
587.02(13)	110.8(19)	120.7(18)	2458.7(3)	1871.7	27/2$^+$	23/2$^+$
643.70(95)	29.1(12)	23.5(9)	4613.9(14)	3970.2	43/2$^+$	39/2$^+$
712.00(95)	26.0(9)	18.3(7)	5325.9(0)	4613.9	47/2$^+$	43/2$^+$
775.80(95)	18.0(8)	8.7(6)	6101.7(0)	5325.9	51/2$^+$	47/2$^+$
974.98(31)	14.0(8)	2.2(4)	9305.7(23)	8330.7	67/2$^+$	63/2$^+$
γ-rays from states in the [402 5/2$^+$] band						
136.10(12)	10.0(10)	10.0(10)	141.5(1)	5.5	7/2$^+$	5/2$^+$
164.28(12)	43.3(16)	62.9(17)	305.7(2)	141.5	9/2$^+$	7/2$^+$
193.80(12)	41.9(11)	124.3(22)	499.4(2)	305.7	11/2$^+$	9/2$^+$
212.17(14)	25.7(9)	41.3(10)	711.4(3)	499.4	13/2$^+$	11/2$^+$
241.82(15)	17.3(6)	25.6(6)	1197.4(4)	955.5	17/2$^+$	15/2$^+$
244.33(15)	17.3(7)	26.0(7)	955.5(4)	711.4	15/2$^+$	13/2$^+$
262.05(18)	11.1(6)	19.3(6)	1740.1(4)	1478.5	21/2$^+$	19/2$^+$
281.10(16)	13.4(6)	19.2(6)	1478.5(5)	1197.4	19/2$^+$	17/2$^+$
300.12(15)	17.4(10)	23.6(10)	305.7(2)	5.5	9/2$^+$	5/2$^+$

Table 1 — continued

E_γ	I_γ,^{31}P	I_γ,^{19}F	E_i	E_f	J_i	J_f
357.56(16)	24.5(9)	29.6(9)	499.4(2)	141.5	$11/2^+$	$7/2^+$
404.85(20)	18.2(10)	18.9(8)	2753.5(6)	2348.6	$29/2^+$	$25/2^+$
405.57(16)	23.0(11)	26.3(9)	711.4(3)	305.7	$13/2^+$	$9/2^+$
436.27(44)	8.0(9)	16.7(8)	955.5(4)	519.7	$15/2^+$	$11/2^+$
448.60(27)	5.9(6)	5.2(5)	1740.1(4)	1292.0	$21/2^+$	$17/2^+$
455.88(18)	24.2(10)	27.8(9)	955.5(4)	499.4	$15/2^+$	$11/2^+$
458.97(15)	40.5(11)	45.3(10)	2753.5(6)	2294.6	$29/2^+$	$25/2^+$
475.01(24)	10.4(6)	11.3(5)	2294.6(4)	1818.4	$25/2^+$	$21/2^+$
486.10(15)	34.7(11)	46.7(10)	1197.4(4)	711.4	$17/2^+$	$13/2^+$
523.49(18)	27.3(13)	34.8(12)	1478.5(5)	955.5	$19/2^+$	$15/2^+$
554.59(15)	33.7(13)	39.4(11)	2294.6(4)	1740.1	$25/2^+$	$21/2^+$
564.03(23)	16.3(9)	22.5(8)	2612.3(14)	2048.3	$27/2^+$	$23/2^+$
569.75(18)	22.9(11)	31.6(9)	2048.3(9)	1478.5	$23/2^+$	$19/2^+$
587.66(95)	6.8(15)	10.6(14)	2753.5(6)	2166.8	$29/2^+$	$25/2^+$
γ-rays from states in the [411 $1/2^+$] band						
147.67(14)	10.0(10)	10.0(10)	147.7(3)	0.0	$5/2^+$	$3/2^+$
195.41(11)	83.3(32)	113.6(43)	195.4(1)	0.0	$7/2^+$	$3/2^+$
214.07(16)	13.2(5)	16.1(5)	519.7(1)	305.7	$11/2^+$	$9/2^+$
231.88(20)	8.5(6)	19.8(6)	943.4(2)	711.4	$15/2^+$	$13/2^+$
237.39(16)	14.9(8)	20.4(9)	432.7(3)	195.4	$9/2^+$	$7/2^+$
284.96(17)	15.2(9)	19.5(9)	432.7(3)	147.7	$9/2^+$	$5/2^+$
301.53(95)	16.3(6)	18.3(6)	821.2(3)	519.7	$13/2^+$	$11/2^+$
324.18(12)	83.2(17)	111.5(18)	519.7(1)	195.4	$11/2^+$	$7/2^+$
348.32(20)	11.0(5)	12.3(5)	1292.0(4)	943.4	$17/2^+$	$15/2^+$
388.46(14)	33.4(10)	36.4(9)	821.2(3)	432.7	$13/2^+$	$9/2^+$
423.70(12)	75.0(13)	88.5(12)	943.4(2)	519.7	$15/2^+$	$11/2^+$
444.10(15)	26.8(8)	29.8(8)	943.4(2)	499.4	$15/2^+$	$11/2^+$
470.89(15)	38.3(11)	45.2(10)	1292.0(4)	821.2	$17/2^+$	$13/2^+$
502.07(12)	98.2(15)	111.3(15)	1445.5(3)	943.4	$19/2^+$	$15/2^+$
526.14(17)	38.0(11)	45.3(10)	1818.4(6)	1292.0	$21/2^+$	$17/2^+$
530.23(20)	18.5(8)	24.6(7)	2348.6(6)	1818.4	$25/2^+$	$21/2^+$
542.58(16)	34.7(11)	43.1(10)	1740.1(4)	1197.4	$21/2^+$	$17/2^+$
544.73(13)	92.9(14)	102.8(13)	1990.2(3)	1445.5	$23/2^+$	$19/2^+$
548.45(15)	36.7(9)	45.3(9)	2538.7(4)	1990.2	$27/2^+$	$23/2^+$
608.84(20)	18.1(10)	19.8(8)	2348.6(6)	1740.1	$25/2^+$	$21/2^+$
γ-rays from states in the [660 $1/2^+$] band						
343.50(32)	10.0(10)	10.0(10)	2222.5(15)	1879.0	$25/2^+$	$21/2^+$
445.28(24)	14.9(9)	15.6(7)	2709.0(7)	2263.7	$29/2^+$	$25/2^+$
445.41(27)	3.8(9)	4.5(6)	2263.7(11)	1818.4	$25/2^+$	$21/2^+$
480.02(40)	6.9(6)	5.7(5)	3233.4(9)	2753.5	$33/2^+$	$29/2^+$
486.38(40)	7.4(8)	10.5(7)	2709.0(7)	2222.5	$29/2^+$	$25/2^+$
523.63(95)	5.0(8)	7.4(10)	2263.7(11)	1740.1	$25/2^+$	$21/2^+$
524.44(20)	11.5(9)	11.0(9)	3233.4(9)	2709.0	$33/2^+$	$29/2^+$
582.36(18)	21.5(11)	25.6(9)	3815.8(12)	3233.4	$37/2^+$	$33/2^+$
696.10(20)	19.7(9)	15.5(7)	5153.2(15)	4457.1	$45/2^+$	$41/2^+$
750.73(20)	20.6(9)	10.8(6)	5903.9(18)	5153.2	$49/2^+$	$45/2^+$
803.52(26)	14.0(7)	6.4(5)	6707.4(22)	5903.9	$53/2^+$	$49/2^+$
855.31(25)	14.9(7)	4.9(4)	7562.7(25)	6707.4	$57/2^+$	$53/2^+$
907.47(34)	9.1(7)	2.6(4)	8470.2(33)	7562.7	$61/2^+$	$57/2^+$
962.30(37)	8.0(7)	2.1(3)	9432.5(40)	8470.2	$65/2^+$	$61/2^+$

Table 1 — continued

E_γ	I_γ,^{31}P	I_γ,^{19}F	E_i	E_f	J_i	J_f
γ-rays from states in the three-quasiparticle band						
235.60(3)	26.5(6)	31.1(6)	3436.7(4)	3201.1	$35/2^+$	$33/2^+$
244.11(14)	25.2(6)	31.0(6)	3201.1(4)	2956.8	$33/2^+$	$31/2^+$
268.63(20)	16.2(6)	18.0(5)	3706.0(8)	3436.7	$37/2^+$	$35/2^+$
275.23(95)	7.1(4)	9.1(4)	3981.3(5)	3706.0	$39/2^+$	$37/2^+$
288.46(15)	10.6(5)	13.4(5)	4270.1(6)	3981.3	$41/2^+$	$39/2^+$
299.85(95)	14.2(5)	12.4(5)	4270.1(6)	3970.2	$41/2^+$	$39/2^+$
309.08(20)	16.3(8)	18.3(8)	4579.5(6)	4270.1	$43/2^+$	$41/2^+$
309.36(15)	38.0(9)	28.9(8)	4888.8(6)	4579.5	$45/2^+$	$43/2^+$
318.58(13)	30.7(5)	21.3(4)	5539.5(7)	5220.8	$49/2^+$	$47/2^+$
331.86(14)	25.0(5)	22.6(5)	5220.8(6)	4888.8	$47/2^+$	$45/2^+$
335.99(14)	22.9(6)	23.8(5)	6236.0(8)	5899.7	$53/2^+$	$51/2^+$
360.06(14)	22.8(5)	13.9(4)	5899.7(7)	5539.5	$51/2^+$	$49/2^+$
365.94(20)	9.1(5)	6.1(4)	6997.6(9)	6632.0	$57/2^+$	$55/2^+$
395.84(18)	13.9(5)	13.7(5)	6632.0(9)	6236.0	$55/2^+$	$53/2^+$
398.62(20)	13.3(6)	11.1(5)	7837.4(11)	7439.0	$61/2^+$	$59/2^+$
441.98(28)	5.9(5)	5.8(4)	7439.0(10)	6997.6	$59/2^+$	$57/2^+$
470.65(18)	32.6(10)	35.6(9)	3201.1(4)	2730.3	$33/2^+$	$29/2^+$
479.83(17)	23.0(8)	27.5(8)	3436.7(4)	2956.8	$35/2^+$	$31/2^+$
493.21(31)	5.2(7)	10.0(6)	8330.7(14)	7837.4	$63/2^+$	$61/2^+$
544.65(15)	33.9(10)	37.3(9)	3981.3(5)	3436.7	$39/2^+$	$35/2^+$
562.48(35)	5.0(7)	6.0(8)	3981.3(5)	3417.3	$39/2^+$	$35/2^+$
564.04(95)	0.0(5)	1.8(5)	4270.1(6)	3706.0	$41/2^+$	$37/2^+$
587.46(21)	14.3(9)	18.1(9)	4270.1(6)	3682.6	$41/2^+$	$37/2^+$
598.55(15)	40.7(10)	38.3(9)	4579.5(6)	3981.3	$43/2^+$	$39/2^+$
609.29(95)	18.9(7)	20.2(7)	4579.5(6)	3970.2	$43/2^+$	$39/2^+$
618.51(15)	44.7(8)	35.7(7)	4888.8(6)	4270.1	$45/2^+$	$41/2^+$
641.44(17)	37.9(11)	33.5(9)	5220.8(6)	4579.5	$47/2^+$	$43/2^+$
651.13(15)	45.3(10)	29.8(8)	5539.5(7)	4888.8	$49/2^+$	$45/2^+$
679.18(18)	24.2(7)	18.4(6)	5899.7(7)	5220.8	$51/2^+$	$47/2^+$
696.73(17)	29.8(9)	20.9(7)	6236.0(8)	5539.5	$53/2^+$	$49/2^+$
732.95(20)	23.6(8)	11.4(6)	6632.0(9)	5899.7	$55/2^+$	$51/2^+$
761.39(18)	31.1(8)	12.6(6)	6997.6(9)	6236.0	$57/2^+$	$53/2^+$
806.93(20)	28.6(9)	9.9(5)	7439.0(10)	6632.0	$59/2^+$	$55/2^+$
839.50(22)	22.1(8)	12.3(6)	7837.4(11)	6997.6	$61/2^+$	$57/2^+$
891.77(25)	17.9(8)	5.3(5)	8330.7(14)	7439.0	$63/2^+$	$59/2^+$
917.66(24)	20.3(8)	3.6(5)	8755.1(16)	7837.4	$65/2^+$	$61/2^+$
974.98(31)	14.0(8)	2.2(4)	9305.7(23)	8330.7	$67/2^+$	$63/2^+$

lished. A short sequence of levels with tentative spin values 21/2 and 25/2, to which the $29/2^+$ state of the [660 $1/2^+$] band decays by a 486 keV transition, could possibly belong to the three-quasiparticle band which is not known below $I = 33/2^+$. A coincidence spectrum obtained by gating on the 445 keV $29/2^+ \rightarrow 25/2^+$ transition, clearly demonstrating the whole band as well as the 445 keV transition to the [411 $1/2^+$] band, is shown in the top part of Fig. 2. It should be noted that the decay pattern shown in Fig. 1 presents a rather firm determination of spin and parity that agrees with the corresponding quantities for the [660 $1/2^+$] band in ^{163}Lu.

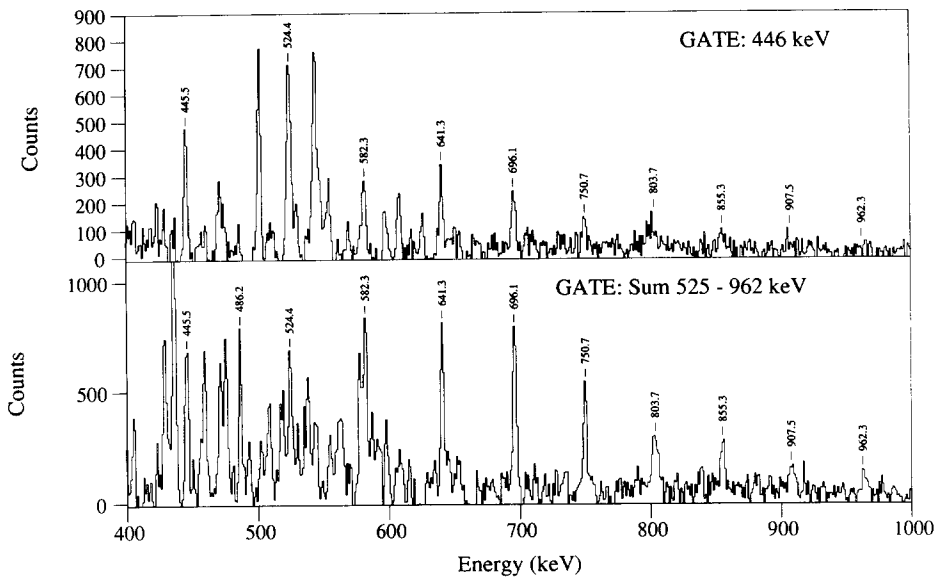

Fig. 2. Spectra of γ-rays related to the new "[660 1/2$^+$]" band in ^{165}Lu. In the lower part is shown a spectrum corresponding to the sum of very narrow gates on all the transitions from 525 to 962 keV. The upper spectrum shows a single gate on the 445.5 keV transition which is found both low in the band and feeding out of the band (self-gating).

The excitation energy versus spin and relative alignment versus rotational frequency for the [660 1/2$^+$] band together with some of the "normal" bands are shown on the right hand side of Fig. 3, which also has the yrast negative parity band, $h_{11/2}$[514 9/2$^-$], included. The corresponding quantities for ^{163}Lu [4] are shown on the left hand side of the figure.

The population of the [660 1/2$^+$] band in ^{165}Lu is around 35% compared to the population of the lowest "normal" positive parity bands with $\alpha = +\frac{1}{2}$. The latter is estimated as half the summed intensity of both signatures in the [404 7/2$^+$] and three-quasiparticle bands in the spin range 41/2–61/2 $\hbar$. The corresponding fraction for ^{163}Lu is around 50% in the same spin range [4]. This population difference could be compatible with the higher excitation energy in ^{165}Lu.

In both nuclei, the [660 1/2$^+$] band begins with a large aligned angular momentum at low frequency, which increases over the entire range, relative to the reference used in Fig. 3. A large aligned angular momentum of $\sim 6\hbar$ is expected for a band built on the [660 1/2$^+$] configuration. The gradual alignment gain is very different from the other bands in the region of the $i_{13/2}$ AB neutron crossing. It can be caused by either a wrongly chosen reference since the deformation is larger for the [660 1/2$^+$] band than for the other bands, or by a much larger interaction strength at the AB crossing, or a combination of both effects. The problem will be addressed in connection with our results from the calculations described below.

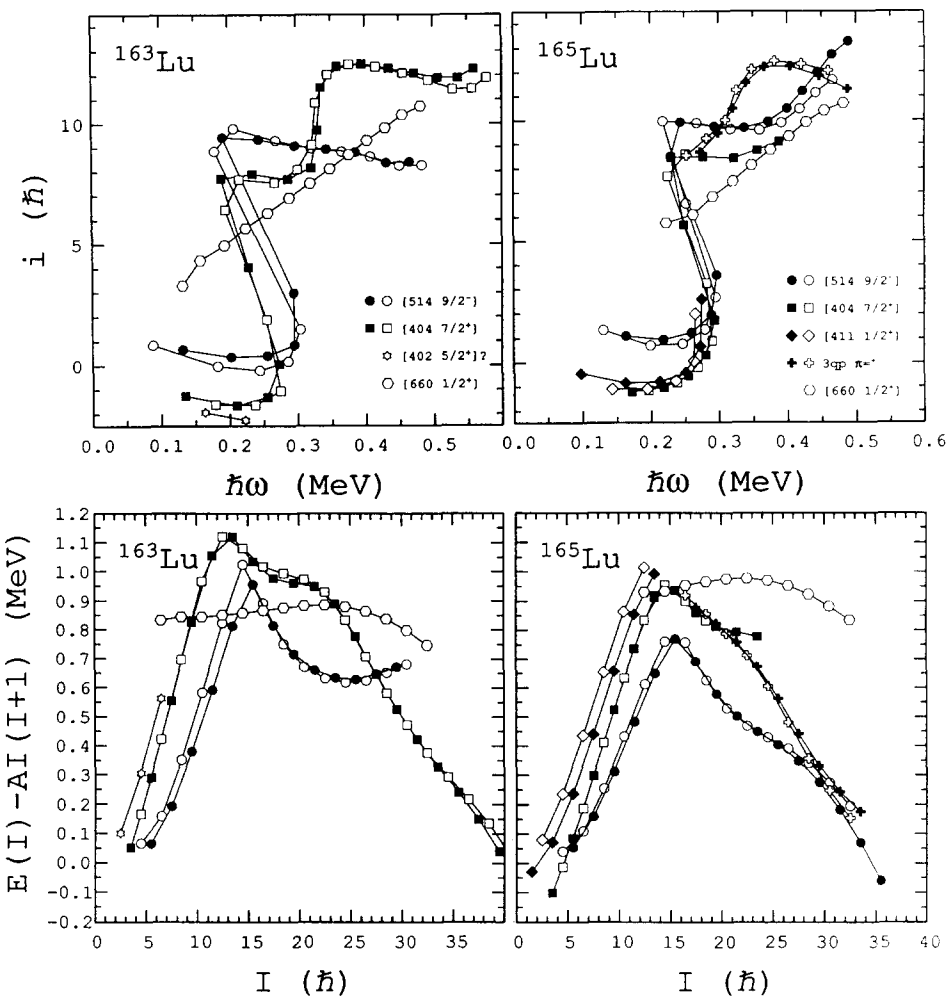

Fig. 3. Experimental properties for selected bands in ^{163}Lu (left) and ^{165}Lu (right). Top: Alignment, i, relative to a reference with Harris parameters $\mathcal{J}_0 = 35\hbar^2$ MeV^{-1} and $\mathcal{J}_1 = 40\hbar^4$ MeV^{-3}, versus rotational frequency. Bottom: Excitation energy relative to a rigid reference with $\mathcal{J} = 63.3\hbar^2$ MeV^{-1} versus spin.

4. Calculations

4.1. Technical details

Comparisons to (adiabatic) TRS calculations, which produce total routhian surfaces for fixed values of the rotational frequency, have been used extensively for assigning configurations to observed rotational bands. The method is attractive to use, since TRS calculations are comparatively easy to perform. However, in the present investigation total energy surfaces (TES) calculated for fixed values of the angular momentum will be used [12]. In its simplest form a TES is adiabatic, just like the TRS, implying

that each energy surface may contain more than one configuration, see Ref. [13]. Therefore, it is often hard to deduce the properties of individual configurations. In such cases it is advantageous to consistently remove weak interactions in such a way that single configurations can be followed diabatically throughout the considered part of the deformation space [13]. This makes it possible to construct diabatic total energy surfaces for individual configurations.

The computer code "Ultimate Cranker" [14] provides the tools for a diabatic treatment of crossings between quasiparticle energy levels with a weak or moderate interaction strength, which is a prerequisite for constructing diabatic energy surfaces. In addition the selected configuration has to be identified at each deformation point. Since the only conserved quantum numbers are parity and signature (π, α), the quasiparticle levels, occupied in a given configuration cannot be automatically identified. Instead the levels are ordered energetically within each symmetry group (π, α) and the ordering numbers of the levels occupied by excited quasiparticles are given as input. However, due to level crossings occurring between the deformation grid points, these numbers are not the same at all grid points. They must therefore be explicitly specified at each deformation point. For excitations to high spin intruder levels, this can be done fairly easily by simply inspecting the quasiparticle energy diagrams, since these levels have a significantly steeper slope than other levels close to the Fermi surface. However, when a large area in deformation space is considered, as in the present investigation, a large number of deformation points has to be processed, which makes the procedure very time consuming. Furthermore, it is in practice not possible to safely determine the identity of the normal parity levels just by inspecting the quasiparticle energy diagrams. Therefore, a more efficient procedure for making configuration assignments is needed. As a direct consequence of the present investigation such a procedure was worked out. It is described in the appendix and was for the first time used in the calculations presented in Ref. [3].

Once a configuration is specified at one rotational frequency, it can in most cases automatically be traced diabatically to higher rotational frequencies, since frequency diabatic quasiparticle energy levels are used in the calculations. However, at certain deformation points a given crossing between two quasiparticle levels may be associated with a large interaction. In such cases the interaction will not be removed, preventing the construction of diabatic configurations through that crossing. This complicates the construction of diabatic energy surfaces over large deformation spaces. Truly diabatic energy surfaces could therefore not be constructed in the present calculations. Surfaces which are diabatic with respect to certain specified level crossings could, however, be constructed.

In all calculations particle number projection is applied. The total energy surfaces (Figs. 4, 5 and 8) and the quasiparticle energy diagrams (Fig. 7) were calculated using a fraction of 80% of the BCS value of the pairing gap Δ at $\omega = 0$ for protons. This value was kept fixed for all frequencies. For neutrons the full BCS value of Δ was used in the case of the 0-quasineutron configuration, whereas 75% of this value was used in the 2-quasineutron case. In the calculation of spin as a function of frequency (Fig. 6),

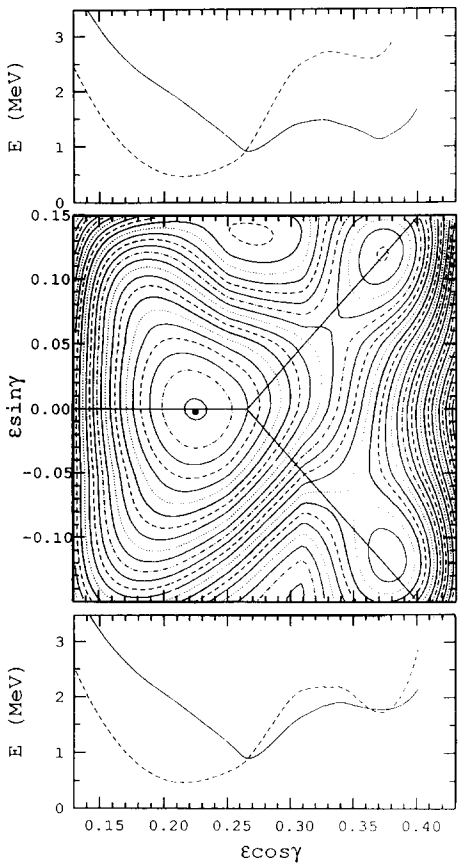

Fig. 4. Center: Lowest spin-adiabatic potential energy surface for $(\pi, \alpha) = (+, +1/2)$ at $I = 14.5$ in ^{165}Lu. The energy difference between contour lines is 0.1 MeV. At the top and bottom are shown the potential energy corresponding to the configuration separated (spin-diabatic) surfaces shown in Fig. 5, as a function of $x = \varepsilon_2 \cos\gamma$ following the straight lines, indicated in the energy surface, cutting through the relative minima with $\gamma > 0$ and $\gamma < 0$, respectively, symmetrically around $\gamma = 0$. The full and broken lines correspond to the [660 1/2$^+$] and the lowest of the [404 7/2$^+$] and [411 1/2$^+$] configurations, respectively.

pairing self-consistency was required. The pairing strength, G, was reduced to 95% in accordance with Ref. [12]. The Fermi level λ was determined by a BSC calculation at $\omega = 0$ and was kept fixed for all frequencies. The hexadecapole deformation parameter ε_4 was in all calculations found by the energy minimalization procedure in an interval $-0.08 < \varepsilon_4 < 0.08$.

4.2. *Coexisting minima in ^{165}Lu and ^{163}Lu*

The lowest spin-adiabatic potential energy-surface [13], with $(\pi, \alpha) = (+, 1/2)$, is shown in the center part of Fig. 4. In addition to a minimum near a normal deformation of $\varepsilon_2 = 0.23$, the surface contains two local minima at large deformation with values of the asymmetry parameter γ, symmetric around $\gamma = 0$. The results are in qualitative

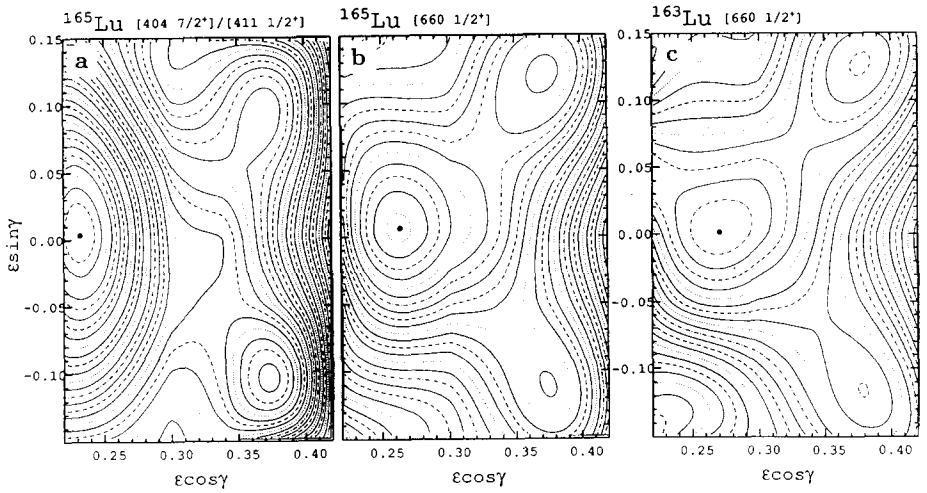

Fig. 5. Configuration separated (spin-diabatic) potential energy surfaces at I = 14.5, corresponding to the [411 1/2$^+$] (along the left margin [404 7/2$^+$]) configuration (a) and the [660 1/2$^+$] configuration (b) in ^{165}Lu, and the configuration separated (spin-diabatic) potential energy surface corresponding to the [660 1/2$^+$] configuration in ^{163}Lu (c). The energy difference between contour lines is 0.1 MeV. The minima found for the [660 1/2$^+$] configuration in ^{165}Lu correspond to (ε_2, γ) = (0.264, 4°) (I), (0.389, +18°) (II) and (0.389, −18°) (III), respectively.

agreement with TRS calculations [4–6] for ^{163}Lu. In the following, these minima are referred to as I, II and III, corresponding to the minimum with normal deformation, large deformation with $\gamma > 0$, and large deformation with $\gamma < 0$, respectively.

In order to highlight the structure of the total energy surface in Fig. 4, partially spin-diabatic energy surfaces are presented in Fig. 5. Due to strong interactions, the first neutron $i_{13/2}$ crossing is treated as an adiabatic crossing in all cases. The surface shown in Fig. 5a corresponds to a configuration in which the odd proton occupies the lowest level above the Fermi surface with N = 4 and $\alpha = +1/2$, combined with the lowest adiabatic neutron configuration with (+,0). At the deformation grid points along the left margin of the surface, the odd proton occupies the [404 7/2$^+$] Nilsson orbital ($g_{7/2}$;4). At the other grid points it occupies the [411 1/2$^+$] orbital ($d_{3/2}$;1). Thus, the main part of the energy surface corresponds to the latter configuration. At the deformation of the absolute energy minimum (min I) the two configurations have nearly the same energy, implying that this minimum lies at a place where the configuration represented in the spin-adiabatic energy surface changes. Without separating the energy surfaces into two diabatic surfaces, corresponding to these two configurations, it is not possible to precisely determine the energy minimum for any of the two configurations, see the discussion in section 3.3 of Ref. [13]. However, such details are not needed for the discussion here.

The features of the energy surface in Fig. 5a are very similar to those of the spin-adiabatic energy surface shown in Fig. 4. Both surfaces have a global minimum at $\varepsilon_2 \approx 0.23$ and two excited minima at large deformations.

The energy surface in Fig. 5b corresponds to the configuration in which the odd proton occupies the lowest [660 1/2$^+$] orbital ($i_{13/2}$;1) at all deformation grid points. It has highly deformed minima at $\varepsilon_2 = 0.389$ with $\gamma \sim \pm 18°$, as in the adiabatic energy surface, but also an energy minimum at $\varepsilon_2 = 0.264$ which is only a slightly larger deformation than that of the ($N = 4$) ground state in Fig. 5a.

Although the energy surfaces in Figs. 5a and 5b are quite similar, there are a few important differences. In the $N = 4$ surface, min III is deeper than min II, whereas in the [660 1/2$^+$] surface the opposite is true. Furthermore, min I is deeper relative to the two other minima in the $N = 4$ surface than in the [660 1/2$^+$] surface. These energy relations are more easily seen in the top and bottom panels in Fig. 4, where the solid curves show the energy of the [660 1/2$^+$] configuration and the dashed curves the energy of the $N = 4$ configuration along the trajectories indicated on top of the spin-adiabatic energy surface in Fig. 4. The energy of this surface along the indicated trajectories is obtained by following the lowest one of the curves in the top and bottom panels, respectively.

Note that the trajectories in Fig. 4 do not correspond exactly to the energetically preferred route through the nonaxial local minima (II and III) for both the $N = 4$ and [660 1/2$^+$] configurations, since these minima are slightly displaced relative to each other, see Fig. 5.

The spin-adiabatic energy surface in Fig. 4 can now be given a more detailed interpretation. It consists of a mixture of the $N = 4$ and [660 1/2$^+$] configurations. At minimum I, the $N = 4$ configuration is lowest, falling below the minimum at $\varepsilon_2 = 0.264$ of the [660 1/2$^+$] configuration, which does not appear as a separate minimum in the spin-adiabatic energy surface of Fig. 4. The reason for this is made obvious by inspecting the top and bottom panels of this figure. At minimum II, the [660 1/2$^+$] configuration is clearly lowest and thus the one represented in the spin-adiabatic energy surface, whereas at minimum III, the $N = 4$ and [660 1/2$^+$] configurations have similar energies and only a closer investigation can tell which one is actually represented in the surface.

In order to make a direct comparison with Refs. [4,6], we have also calculated the energy surface for the [660 1/2$^+$] band in ^{163}Lu, shown in Fig. 5c. It is very similar to the corresponding surface in ^{165}Lu and in qualitative agreement with the TRS surfaces calculated for ^{163}Lu [6]. It should be observed that the highly deformed energy minima have lower energies in ^{163}Lu than in ^{165}Lu, in agreement with the experimental data, cf. Fig. 3.

4.3. Comparison to experimental data

The above analysis has shown that three energy minima are expected. Therefore, one might expect three independent low-lying rotational bands with the odd proton in the lowest $i_{13/2}$ level. However, only one such band is observed. Comparisons with ^{163}Lu, in which the quadrupole moment has been measured for the corresponding band [5], and with calculations, clearly show that the deformation must be large, probably very close

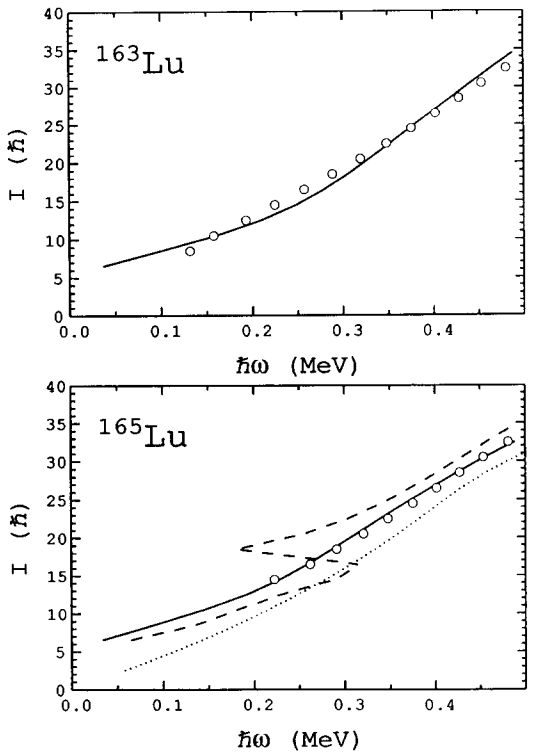

Fig. 6. Lower: Experimental (open circles) and calculated spin versus rotational frequency for the three different minima found in the total energy surface for the [660 1/2$^+$] band in ^{165}Lu. The short-dashed line corresponds to the less deformed minimum (min I), the full and dotted lines correspond to the well deformed minima with $\gamma > 0$ (min II) and $\gamma < 0$ (min III), respectively. Upper: Experimental (open circles) and calculated (full line) spin versus rotational frequency for the well deformed minimum with $\gamma > 0$ in the total energy surface for the [660 1/2$^+$] band in ^{163}Lu.

to the calculated one at $\varepsilon_2 = 0.389$ (min II). The calculated energies, however, are such that the less deformed minimum at $\varepsilon_2 = 0.264$ (min I) is predicted to have the lowest energy and, thus, expected to be the one which should be observed. The difference in energy between min II and min I is, however, only about 200 keV, which is of the same order as the uncertainty in the calculations, cf. Ref. [13]. The minimum at $\gamma \approx -18°$ (min III) has a clearly higher energy than the other two minima.

As a further test of the shape parameters for the different minima, the theoretical relation between spin and rotational frequency, obtained from pairing self-consistent cranking calculations for the [660 1/2$^+$] band, is presented together with the measured values in Fig. 6. The calculated relation between I and ω at the well deformed minimum with $\gamma > 0$ (min II) shows for both of the two neighbouring even-N Lu isotopes a very similar gradual increase with ω, in qualitative agreement with the data. The calculated results for the other minima found in ^{165}Lu are also shown in the lower part of Fig. 6. For the normally deformed minimum with $(\varepsilon_2, \gamma) = (0.264, \sim 0)$ (min. I) the $i_{13/2}$ neutron crossing is clearly seen as a backbending, in contrast to the data.

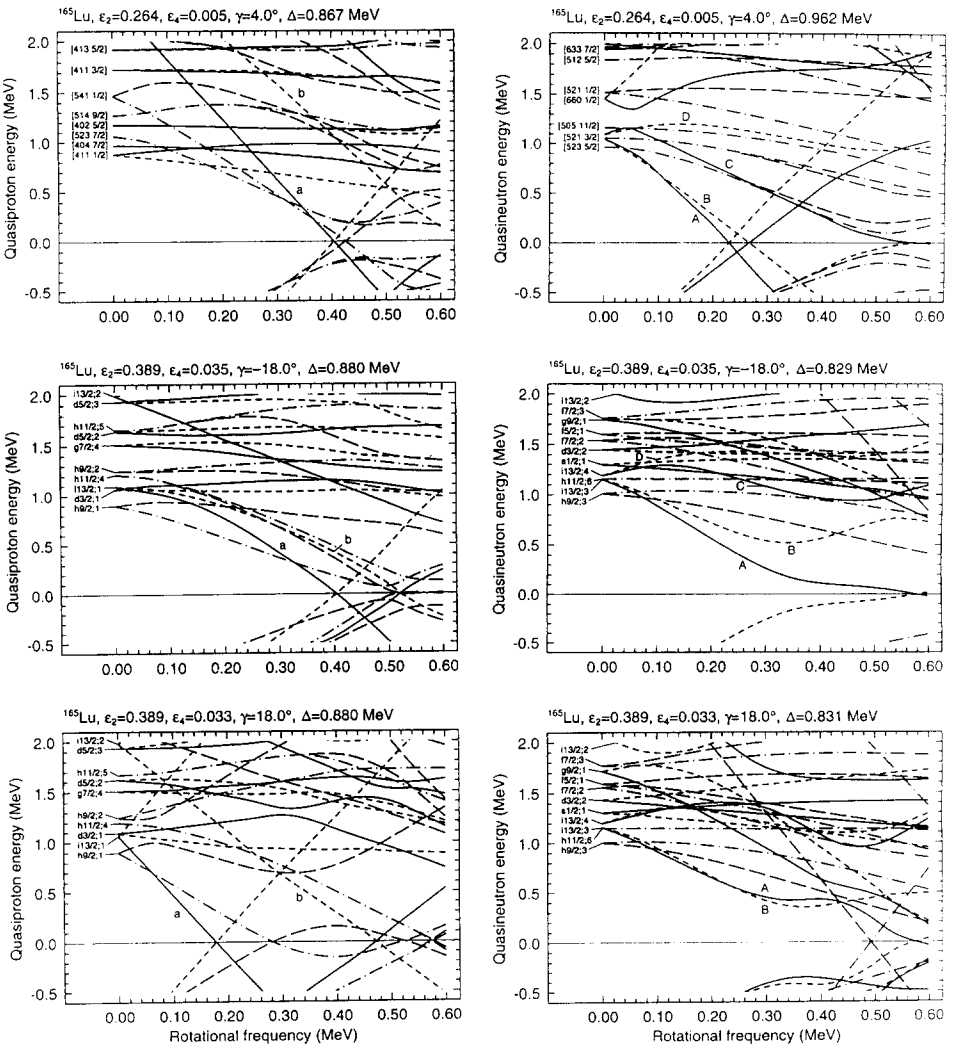

Fig. 7. Calculated quasiparticle energy diagrams for protons and neutrons at the three minima in the total energy surface shown in Fig. 5b, corresponding to the $i_{13/2}[660\ 1/2^+]$ configuration in ^{165}Lu.

In Fig. 7, routhian diagrams for both quasiprotons (left) and quasineutrons (right) corresponding to the deformations of the three minima, are presented. From the calculation corresponding to the deformation $(\varepsilon_2, \gamma) = (0.389, +18°)$ (min. II) one may conclude that a pair of quasineutrons is aligned at the highest spin and that the $i_{13/2}$ neutron crossing occurs with a very large interaction.

Furthermore, at min II the alignment of a pair of $h_{9/2}$ protons occurs at $\hbar\omega \sim 0.35$ also with a large interaction, cf. Fig. 7. The bandcrossing in the $[660\ 1/2^+]$ band is therefore expected to be rather complex, which may explain the observed similarity between the two neighbouring nuclei with neutron numbers 92 and 94, for which the

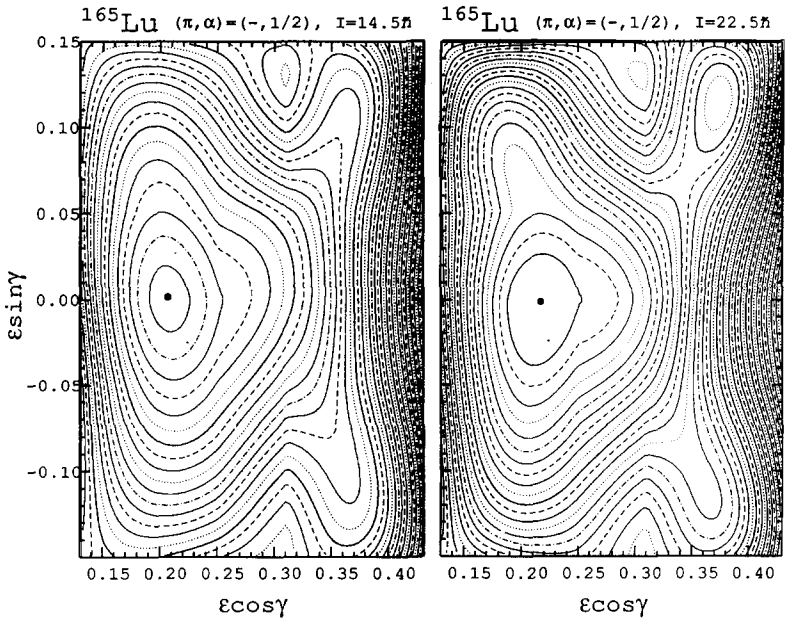

Fig. 8. Spin-adiabatic potential energy surface for the lowest $(-,+1/2)$ configuration in ^{165}Lu, for $I = 14.5$ $\hbar$ (left) and $I = 22.5$ $\hbar$ (right).

interaction strength in a pure crossing caused by the alignment of a pair of $i_{13/2}$ neutrons is expected to depend on the neutron number.

5. Interpretation of the structures in the total energy surfaces

5.1. Basic shell structures

The appearance of energy minima with a very large deformation for the normal parity configuration with $N = 4$ (Fig. 5a) is somewhat surprising. The deformation is so large that it can be classified as superdeformed. One would then expect that at least some levels from higher-lying shells should be occupied. In the $N = 4$ configuration, this is not the case, except for about 0.6 particles scattered into the proton $i_{13/2}$ subshell by the pairing correlations. Actually, the appearance of energy minima at large deformation in ^{165}Lu is a general phenomenon, appearing in all configurations. To demonstrate this, we show in Fig. 8 the spin-adiabatic energy surface at two different spins for the lowest configuration with $(\pi, \alpha) = (-,+1/2)$. Compared to the energy surface in Fig. 4, the role of the configurations [660 $1/2^+$] and [404 $7/2^+$]/[411 $1/2^+$] is here replaced by the negative parity (semi)-intruder $h_{9/2}$[541 $1/2^-$] and the normal parity $h_{11/2}$[514 $9/2^-$] configurations.

We can therefore conclude that the appearance of coexisting minima at large and normal deformations is not the result of placing the odd proton in different orbitals, since these minima appear consistently, independent of which orbital is occupied by

the odd proton, including the strongly downsloping orbitals [660 1/2] and [541 1/2] and strongly upsloping orbitals like [404 7/2]. Thus, the different shapes are not the result of polarizing effects of the odd proton. A measure of the strength of the polarization effect of a proton in the [660 1/2] orbital is provided by comparing the [660 1/2] minimum at $\varepsilon_2 = 0.264$ with the less deformed minimum of the mixed [404 7/2]/[411 1/2] configuration at $\varepsilon_2 = 0.23$ and the change in triaxiality from $\pm 16.4°$ in the [411 1/2] configuration to $\pm 18°$ in the [660 1/2] configuration for minima II and III. The explanation to the coexisting minima must therefore involve more profound shell structures, which are only marginally affected by the particular proton configuration.

Favourable shell structures in the *proton system* are produced both at $\varepsilon_2 \approx 0.23$, when the upsloping orbitals [404 7/2] ($g_{7/2}$;4) and [402 5/2] ($d_{5/2}$;3) are near the Fermi surface, see Fig. 9, and the pairing scatters particles into these orbitals at a low cost of energy, and at larger deformations with, $\varepsilon_2 \approx 0.39$, where the downsloping orbitals [660 1/2] ($i_{13/2}$;1) and [541 1/2] ($h_{9/2}$;1) are near the Fermi surface and partially occupied. At intermediate deformations both kinds of orbitals are higher in energy and the total energy unfavourable, since at least one (the number depends on the configuration) of these levels has to be occupied.

The most important shell structure is, however, found in the *neutron system*, where a major shell gap appears at $N = 94$ at the deformations appropriate for minimum II and III. Appearing at a highly deformed triaxial shape, this gap is exceptionally large, almost as large as the spherical gap at $N = 64$. It guarantees the appearance of energy minima at these shapes, regardless of the proton configuration. The energy gap belongs to a family of superdeformed ($\varepsilon_2 \approx 0.4 - 0.5$) highly triaxial ($\gamma \approx 20°$) shell structures, predicted to generate low-lying coexisting energy minima for certain favourable combinations of proton and neutron numbers [16]. One such combination is $Z \approx 70$ and $N \approx 90$, which is closely matching the Lu isotopes studied here. The [660 1/2] bands in ^{163}Lu and ^{165}Lu are the first bands belonging to this family, which have been experimentally observed.

5.2. *Structural differences between different energy minima*

The structural difference between energy minima at various shapes can be illustrated by calculating the occupation numbers for the individual single-particle levels. However, such calculations become meaningful only if the single-particle levels can be labeled in a unique way, independent of deformation and rotational frequency. Preferably, the labels should be both informative and simple to assign. How such labels can be determined, based on the quantum numbers N, ℓ and j, is described in the appendix. These labels have been used in Figs. 7 and 9 and will also be used in this subsection.

When the deformation is changed from the smaller one (min I) to any of the larger ones (min II or III), particles are transferred away from the $N = 4$ shell, notably from the upsloping $g_{7/2}$;4 and $d_{5/2}$;3 levels, into downsloping levels from the $h_{9/2}$, $f_{7/2}$ and $i_{13/2}$ subshells.

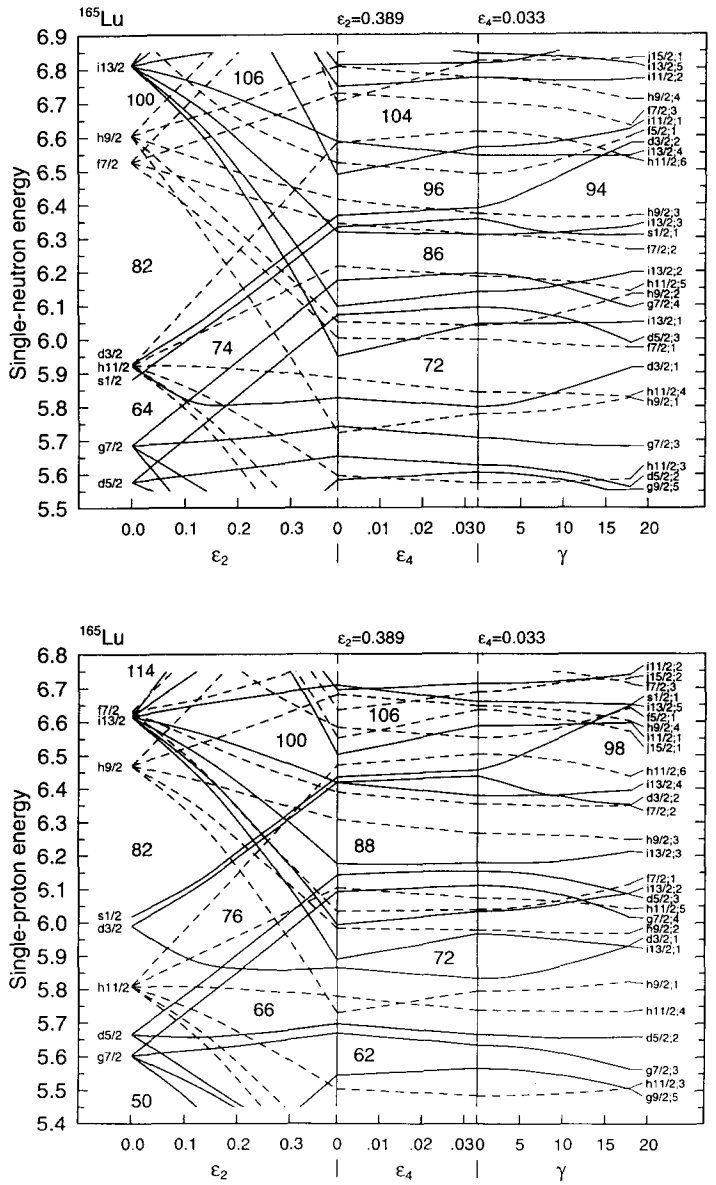

Fig. 9. Single-particle energies as functions of deformation. In the left part the quadrupole deformation increases from $\varepsilon_2 = 0.0$ to $\varepsilon = 0_2.389$. In the middle part the quadrupole deformation is $\varepsilon_2 = 0.389$ and the hexadecapole deformation increases from $\varepsilon_4 = 0.0$ to $\varepsilon_4 = 0.033$. In the right part $\varepsilon_2 = 0.389$ and $\varepsilon_4 = 0.033$ and the triaxiality increases from $\gamma = 0.0°$ to $\gamma = 18.0°$. The neutron energies are shown in the top diagram and the proton energies in the bottom diagram. Solid lines indicate positive parity ($N = 4$, except for the $i_{13/2}$ and $i_{11/2}$ levels, which have $N = 6$) and dashed lines negative parity ($N = 5$, except for the $j_{15/2}$ levels, which have $N = 7$). The potential parameters used are those of Ref. [15].

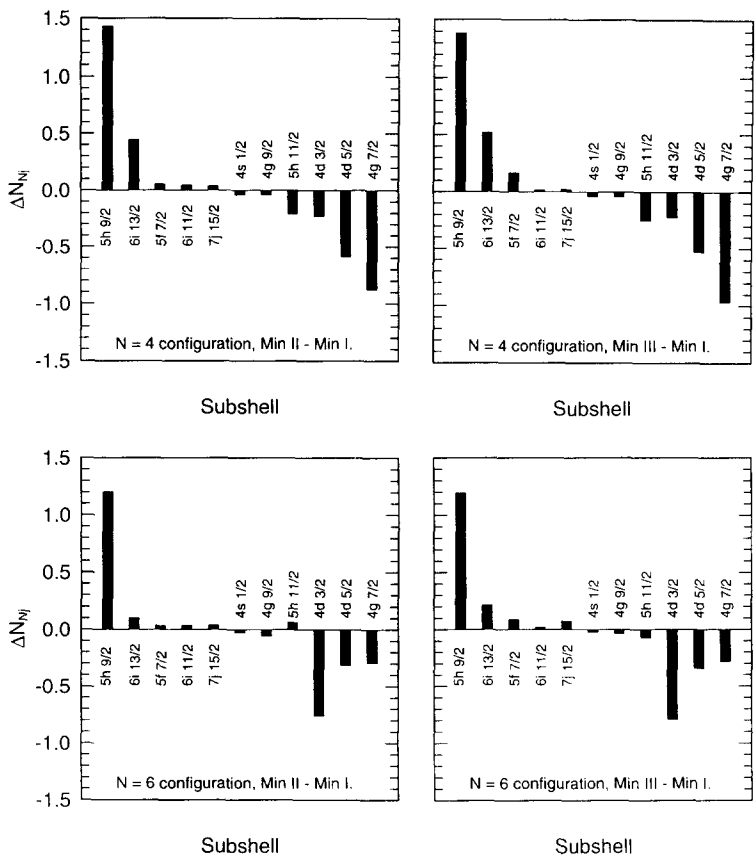

Fig. 10. Differences in subshell occupation between the local minima II (left) and III (right) and the global minimum (I) at the rotational frequency $\hbar\omega = 0.25$ MeV for the $N = 4$ configuration [411 1/2] (top) and the $N = 6$ configuration [660 1/2] (bottom). The subshells are characterized by quantum numbers $N\ell j$.

In the $N = 4$ band, here identified with the $d_{3/2}$;1 ([411 1/2]) configuration, the $g_{7/2}$ subshell is losing nearly one particle, mainly from the $g_{7/2}$;4 ([404 7/2]) orbital, and the $d_{5/2}$ subshell about 0.5 particles, mainly from the $d_{5/2}$;3 ([402 5/2]) orbital. Most of the particles are absorbed by the lowest $h_{9/2}$ and $f_{7/2}$ orbitals, in total about 1.5 particles, and about 0.5 particles go into the $i_{13/2}$ subshell, see Fig. 10.

In the configuration in which the odd proton occupies the $i_{13/2}$;1 ([660 1/2]) level, this level is blocked and the occupation number for the $i_{13/2}$ subshell is close to one at all deformation grid points. On the other hand, the $d_{3/2}$;1 level is not blocked, as it was in the previous configuration, allowing particles to be efficiently scattered out of the $d_{3/2}$ subshell, in total about 0.8 particles. Fewer particles are scattered out of the $g_{7/2}$ and $d_{5/2}$ subshells, only about 0.3 from each. The explanation to these low numbers is the larger deformation ($\varepsilon_2 = 0.264$) of min I in the $i_{13/2}$;1 configuration compared to the one in the $d_{3/2}$;1 configuration ($\varepsilon_2 = 0.235$), which gives a lower filling of the $g_{7/2}$ and $d_{5/2}$ subshells already at min I. The difference is about half a particle in each of

the two subshells. Most of the particles are absorbed by the $h_{9/2}$ subshell.

It should be observed that the occupation of the different subshells is nearly identical at the large deformations with $\gamma = 16.4°$ and $\gamma = -16.4°$ in the [411 1/2] configuration and with $\gamma = 18°$ and $\gamma = -18°$ in the [660 1/2] configuration. This is not surprising, since these shapes are identical and for $\omega = 0$ the wave functions are exactly equal. Differences appear only for $\omega > 0$.

Also in the neutron system important structural changes take place as the deformation is increased from min I to min II or III. Mainly, particles are scattered out of the $h_{11/2}$ and $d_{3/2}$ subshells into the $h_{9/2}$ and $i_{13/2}$ subshells.

5.3. *The spin orientation*

Although the shape is the same in minimum II and minimum III, different cranking axes are used in the two cases, and therefore the wave functions gradually diverge as the rotational frequency increases, leading to completely orthogonal states already at low ω values. This does, however, only marginally change the distribution on the different subshells, but influences strongly the distribution over the different magnetic substates, leading to very different ways of building up angular momentum. This is exemplified in Fig. 11, showing the distribution on different projection quantum numbers Ω_x along the rotational axis for the $i_{13/2}$;1 quasiparticle level with positive signature ($\alpha = 1/2$), which is the level occupied by the odd proton in the [660 1/2] band. Both in minimum I and minimum II, the angular momentum is strongly aligned along the rotational axis, resulting in large amplitudes only for the $\Omega_x = 13/2$ and $\Omega_x = 9/2$ components. In minimum III no strong alignment appears and the wave function is spread over several Ω_x values. Thus, compared to minimum II, minimum I differs by having a different distribution of particles over the different subshells, see Fig. 10, and minimum III by having a different aligned angular momentum and thus a different distribution over the Ω_x values, see Fig. 11.

5.4. *A case for 3D cranking*

The two highly deformed minima have practically the same shape, implying that one can come from one minimum to the other, not only by moving through the γ plane, but also by tilting the cranking axis and thus not changing the shape. The crucial question is how the energy depends on the tilting angles.

Does the energy have a maximum, leaving the two minima seen in the γ plane as stable minima also with respect to the tilting angles? Or does it slope down as a monotonously decreasing function from the higher minimum to the lower minimum, leaving the higher minimum in the γ plane as a maximum with respect to the tilting angles? Or is there an absolute energy minimum for some intermediate values of the tilting angles, which would then be the only stable high deformation minimum, possibly with a lower energy than that of the less deformed minimum at $\varepsilon_2 = 0.264$?

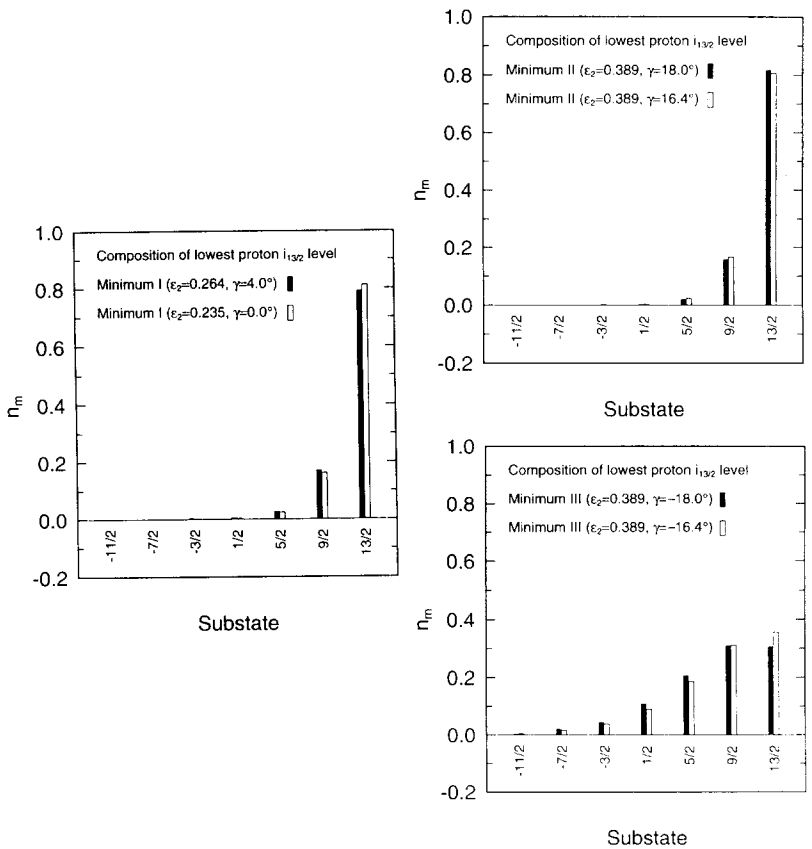

Fig. 11. Composition of the wave function for the $i_{13/2}$;1 $\alpha = 1/2$ quasiparticle level with respect to the spin projection Ω_x along the rotational axis at the rotational frequency $\hbar\omega = 0.25$ MeV. Results are presented for the deformations corresponding to the three energy minima in the total energy surfaces. Full and open bars correspond to the minima found for the [660 $1/2^+$] configuration and for the lowest $N = 4$ configuration, respectively.

To answer the above questions, full scale tilted cranking calculations are required. Since γ is large in this case, a two-dimensional cranking like in Ref. [17] will not be sufficient, because it cannot be guaranteed a priori that the cranking axis will stay in one of the principal planes for all low-lying configurations. General arguments for this can be found in Ref. [18]. Therefore, ^{165}Lu would be one of the most interesting cases to which the three-dimensional cranking described in Refs. [18,19] could be applied.

5.5. *Comparisons with other nuclei*

There are obvious similarities between ^{163,165}Lu and the Re isotopes in the mechanism that produces coexisting shapes in the sense that essentially the same proton orbitals are being depopulated (notably [404 7/2] and [402 5/2]) and populated (in particular [541 1/2]) as the deformation increases [20]. In Re the coexisting bands are often

referred to as g-band and d-band [21].

There are, however, also large differences. In the Re isotopes, the deformation change is much smaller, highly triaxial shapes do not appear and a smaller number of subshells are significantly changing their occupation. In particular, there is only one important receptor subshell, namely $h_{9/2}$. Therefore, an odd proton in the $h_{9/2}$ subshell can completely block the shape coexistence, whereas in Lu no individual odd particle can change the overall pattern of coexisting shapes.

The same shell structure, which produces the highly deformed energy minima in the two Lu isotopes investigated here, should manifest itself in neighbouring nuclei as well [16].

6. Conclusion

We have performed an experimental investigation of the nucleus, ^{165}Lu. Several transitions have been added to the existing level scheme [10,11]. A new band, presumably of three-quasiparticle nature is found to take over a large fraction of the population of the positive parity bands at higher spin. Furthermore, most interestingly we have established a band, which has transition energies very close to the assumed [660 $1/2^+$] band in ^{163}Lu. This latter new band is most naturally interpreted to have the same structure as its partner in ^{163}Lu and is classified as a superdeformed triaxial band.

A theoretical analysis of the structure of the two Lu isotopes, ^{165}Lu and ^{163}Lu has been carried out by detailed calculations of total potential energy surfaces for specific configurations. The calculations are performed by using the cranking model, following the procedure described in Refs. [12,13]. By a diabatic treatment of specific crossings, proton configurations, such as $i_{13/2}$[660 $1/2^+$], are identified throughout the deformation space and as a function of spin. It is found as a general feature that highly deformed local minima of considerable axial asymmetry coexist with a normally deformed global minimum. The depth of these local minima depends on the configuration. The structure of the different global and local minima found in these surfaces is analysed and discussed in terms of the occupation of different subshells.

An investigation of the wave functions at the minima of the potential energy surfaces indicate a complex structure of the highly deformed bands involving changes in the occupation of several subshells for both neutrons and protons as compared to normal deformations. In the proton system particles are transferred mainly from upsloping $N = 4$ levels into down-sloping intruder levels, in particular those originating from the $h_{9/2}$ and $i_{13/2}$ subshells, which are also responsible for shape coexistence in a large number of nuclei from Re to Pb. The difference between the wave functions for the two well deformed local minima with opposite sign in γ is found in a difference in the occupation of the Ω_x components, reflecting different mechanisms for building up angular momentum along the rotational axis.

As demonstrated, nonaxial, highly deformed local minima seem to appear as a general phenomenon. It is related to the appearance of favourable shell structures at superde-

formed triaxial shapes discussed in Ref. [16]. To verify the predicted sizeable divergence from axial symmetry is a challenge for further experiments, as well as theoretical studies of possible measurable spectroscopic consequences.

Acknowledgements

This work has been supported by the Danish Natural Science Foundation, the NORDBALL collaboration and the Swedish Natural Science Research Council. The availability of software written by D.C. Radford used in the data analysis is highly appreciated.

Appendix A

A.1. Labeling of single-particle levels

Usually, the single-particle levels are labeled by their Nilsson labels $[N, n_z, \Lambda, \Omega]$, which in non-rotating axially symmetric nuclei constitute the dominant component of the wave function for most of the levels [22]. However, both Λ and Ω get strongly mixed at triaxial shapes and the rotation mixes severely all the quantum numbers except N, which remains relatively pure. As a result, the Nilsson labels become less appropriate at large triaxial shapes and high rotational frequencies. As a complement to the standard Nilsson labels $[N, n_z, \Lambda, \Omega]$, the spherical subshell notations $[N, \ell, j]$ are often used to label levels originating from a particular spherical subshell. They are particularly useful for the intruder subshells, which have relatively pure values of N, ℓ and j also at triaxial shapes and high rotational frequencies. Only the fourth quantum number, Ω, is strongly mixed. The full structural information is of course contained in the wave functions. However, in the present calculations, as in most calculations involving strongly deformed mean fields, a stretched (i.e. deformation dependent) basis is used [23]. Therefore, different basis states are used at different deformations and a direct comparison is not possible, unless the wave functions are transformed to a common basis. If the shape of the nucleus deviates much from that used for defining the stretching of the basis, the structure of the wave function gets more complex, spreading significantly over several N-shells. For practical applications it would be much more useful if a single well-defined label could be assigned to each single-particle level without having to invoke a complete analysis of the wave function. For this purpose, we shall adopt a simple way of assigning labels without actually having to analyze the wave functions in any detail. These labels are simply given by the spherical subshell quantum numbers $[N, \ell, j]$ that can be assigned to a level by following its diabatic continuation back to spherical shape. To distinguish different levels originating from the same subshell, an ordering number is added. It is given the value 1 for the lowest level and increases in steps of one to $j + 1/2$ for the highest level. Thus the doubly degenerate time reversed levels are given the same label. If a distinction is needed, e.g. when the levels split up as a result of rotation, this is

achieved by adding the signature quantum number, α. The principle for the labeling is illustrated in Fig. 9 and is easily understood by comparing the labels to the right with the notations for the spherical subshells from which the levels originate. Assigning labels this way requires that diabatic levels can be constructed in a unique way. This is not always possible, since there are places in the deformation space, where diabatic continuations are difficult to define. However, for $\varepsilon_2 < 0.4$ and $|\gamma| < 20°$, diabatic levels can nearly always be constructed in a unique way. They can therefore be labelled by effective $[N, \ell, j]$ quantum numbers, which can be used for level classification, as illustrated in Fig. 9.

A.2. The relation between labels and wave functions

Although the subshells may become heavily mixed as deformation and rotational frequency increase, an analysis of the wave functions shows that the effective $[N, \ell, j]$ quantum numbers, determined in accordance to the prescription above, in general are very appropriate, in particular for the high-j subshells, as shown in Table A.1. The table lists all the single-proton levels included in Fig. 9. The squared amplitude of the label component in the wave function is given for three different deformations corresponding to the lowest energy minimum in the $N = 4$ configuration ($\varepsilon_2 = 0.235$, $\varepsilon_4 = 0.017$, $\gamma = 0°$), a large axially symmetric deformation ($\varepsilon_2 = 0.389$, $\varepsilon_4 = 0.033$, $\gamma = 0°$) and the triaxial energy minimum II in the [660 1/2] configuration ($\varepsilon_2 = 0.389$, $\varepsilon_4 = 0.033$, $\gamma = 18°$). At the axially symmetric shapes, the label component is the largest one for all the levels. It is, however, smaller than 0.5 for one level at the smaller deformation and for three levels at the larger deformation. At the highly deformed triaxial deformation, the wave function is less pure, but the label component is still the largest component in the wave function for all levels except three (the ones marked with a black bullet). A comparison with Ref. [23] shows that at normal deformations $[N, \ell, j, \Omega]$ are at least as good quantum numbers as $[N, n_z, \Lambda, \Omega]$. This is hardly surprising since normal deformations of deformed nuclei lie in a transitional region between spherical shapes where $[N, \ell, j, \Omega]$ are the conserved quantum numbers and very deformed shapes at which $[N, n_z, \Lambda, \Omega]$ are the more appropriate quantum numbers.

At the deformations considered here, the dominating components in the wave function, when expressed in the stretched bases, have the N, ℓ and j values given by the label, contributing with more than 50% for the large majority of levels and for the high-j subshells usually with more than 70%. Actually, these quantum numbers are so well preserved that they can be used for automatically tracing a variety of diabatic configurations through considerable regions of the deformation space without ever having to trace the diabatic levels back to spherical shape. This technique was for the first time used in Ref. [3].

Table A.1
Unpaired wave functions
Energy, e_i, and squared amplitude, a^2, of the label component in the proton wave function at $\hbar\omega = 0.0$ MeV, given for three different deformations. Left: $(\varepsilon_2, \varepsilon_4, \gamma) = (0.235, 0.017, 0°)$, middle: $(\varepsilon_2, \varepsilon_4, \gamma) = (0.389, 0.033, 0°)$ and right: $(\varepsilon_2, \varepsilon_4, \gamma) = (0.389, 0.033, 18°)$

Level	e_i	a^2	e_i	a^2	e_i	a^2
$4g_{9/2}$; 5	5.346	1.000	5.566	0.999	5.506	0.932
$4g_{7/2}$; 3	5.619	0.938	5.634	0.920	5.565	0.553
4	5.906	0.989	6.112	0.976	6.015	0.652
$4d_{5/2}$; 2	5.652	0.795	5.666	0.719	5.659	0.437○
3	5.958	0.931	6.154	0.678	6.085	0.560
$4d_{3/2}$; 1	5.843	0.554	5.834	0.464○	5.933	0.323○
2	6.243	0.894	6.438	0.842	6.353	0.417○
$4s_{1/2}$; 1	6.260	0.558	6.456	0.620	6.649	0.309●
$5h_{11/2}$; 3	5.637	0.948	5.485	0.886	5.508	0.854
4	5.778	0.973	5.737	0.945	5.735	0.912
5	5.971	0.992	6.072	0.983	6.041	0.944
6	6.223	1.000	6.502	0.998	6.435	0.953
$5h_{9/2}$; 1	6.123	0.792	5.792	0.539	5.822	0.630
2	6.203	0.842	5.977	0.724	5.968	0.492○
3	6.356	0.916	6.266	0.865	6.248	0.724
4	6.575	0.970	6.645	0.951	6.600	0.844
$5f_{7/2}$; 1	6.295	0.617	6.036	0.332○	6.113	0.246●
2	6.457	0.766	6.350	0.601	6.347	0.495○
3	6.697	0.896	6.750	0.669	6.709	0.614
$5f_{5/2}$; 1	6.711	0.439○	6.548	0.278○	6.637	0.209●
$6i_{13/2}$; 1	6.268	0.765	5.967	0.774	5.931	0.851
2	6.303	0.920	6.034	0.810	6.089	0.816
3	6.377	0.939	6.180	0.810	6.214	0.824
4	6.493	0.960	6.379	0.912	6.395	0.879
5	6.652	0.980	6.660	0.956	6.650	0.924
$6i_{11/2}$; 1	6.940	0.849	6.589	0.622	6.593	0.737
2	6.996	0.866	6.713	0.714	6.739	0.521
$7j_{15/2}$; 1	6.954	0.920	6.636	0.775	6.571	0.868
2	6.984	0.919	6.688	0.818	6.741	0.799

○: Label corresponds to largest component but $a^2 < 0.5$.
●: Label does not correspond to largest component.

A.3. Labeling of quasiparticle levels

The single-particle labels introduced above are also very convenient to use for labeling the quasiparticle levels and have been used as labels in Fig. 7 for the highly triaxial deformations with $\gamma = \pm 18°$, where the ordinary Nilsson labels, $[N, n_z, \Lambda, \Omega]$, are not appropriate. The same ordering number as was assigned to the single-particle levels is

Table A.2
Paired wave functions
Energy, e_i, and squared amplitude, a^2, of the label component in the proton wave function at $\hbar\omega = 0.25$ MeV for two different deformations

Level	$(\varepsilon_2, \varepsilon_4, \gamma) = (0.235, 0.017, 0°)$				$(\varepsilon_2, \varepsilon_4, \gamma) = (0.389, 0.033, 18°)$			
	$\alpha = 1/2$		$\alpha = -1/2$		$\alpha = 1/2$		$\alpha = -1/2$	
	e_i	a^2	e_i	a^2	e_i	a^2	e_i	a^2
$4g_{9/2}$; 1	−9.118	0.907	−8.434	0.918	−10.715	0.848	−9.312	0.774
2	−7.857	0.925	−7.404	0.905	−8.461	0.757	−8.695	0.811
3	−6.805	0.943	−6.745	0.926	−7.220	0.880	−7.221	0.859
4	−5.587	0.981	−5.589	0.981	−5.202	0.925	−5.208	0.916
5	−3.897	0.999	−3.897	0.998	−2.532	0.913	−2.536	0.924
$4g_{7/2}$; 5	−4.501	0.432○	−5.013	0.762	−5.915	0.351○	−6.485	0.651
2	−3.310	0.681	−3.551	0.782	−4.483	0.594	−4.576	0.454○
3	−2.088	0.634	−2.088	0.787	−2.124	0.458○	−2.235	0.475○
4	−0.783	0.871	−0.783	0.872	−1.478	0.679	−1.573	0.560
$4d_{5/2}$; 2	−3.769	0.342●	−3.316	0.581	−3.801	0.197●	−3.383	0.260●
2	−1.834	0.655	−1.832	0.648	−1.568	0.490○	−1.405	0.359●
3	−0.976	0.806	−0.961	0.580	−2.098	0.651	−1.984	0.497○
$4d_{3/2}$; 1	−0.742	0.554	−0.998	0.317●	−0.940	0.331○	−1.238	0.314○
2	−2.685	0.776	−2.633	0.628	−3.760	0.392	−3.932	0.432
$4s_{1/2}$; 1	−2.901	0.592	−2.859	0.375●	−6.068	0.258●	−5.815	0.306●
$5h_{11/2}$; 1	−3.414	0.921	−4.072	0.901	−3.439	0.781	−5.923	0.872
2	−2.293	0.939	−2.820	0.935	−4.427	0.843	−3.397	0.783
3	−1.592	0.928	−1.842	0.946	−2.471	0.846	−2.460	0.820
4	−0.530	0.973	−0.532	0.975	−0.878	0.920	−0.877	0.920
5	−1.160	0.963	−1.191	0.971	−1.806	0.647	−1.813	0.928
6	−2.656	0.997	−2.651	0.997	−4.464	0.955	−4.464	0.954
$5h_{9/2}$; 1	−1.737	0.786	−1.046	0.852	−0.734	0.426○	−0.088	0.669
2	−2.843	0.756	−2.398	0.849	−1.817	0.475○	−1.549	0.469○
3	−3.600	0.854	−3.579	0.880	−3.186	0.760	−3.116	0.637
4	−5.085	0.951	−5.085	0.951	−5.643	0.853	−5.627	0.809
5	−7.098	0.986	−7.098	0.986	−8.776	0.886	−8.768	0.880
$5f_{7/2}$; 1	−2.453	0.574	−3.206	0.635	−1.687	0.242●	−2.348	0.275○
2	−4.202	0.730	−4.281	0.688	−3.817	0.453○	−3.854	0.483○
3	−5.920	0.854	−5.922	0.868	−6.358	0.475○	−6.444	0.643
4	−8.088	0.949	−8.092	0.943	−9.736	0.719	−9.759	0.723
$5f_{5/2}$; 1	−6.087	0.370○	−5.723	0.513	−5.988	0.192●	−5.588	0.248○
2	−8.089	0.667	−8.137	0.741	−8.414	0.437○	−8.242	0.397○
$6i_{13/2}$; 1	−2.095	0.756	−1.435	0.924	−2.539	0.795	0.426	0.874
2	−3.286	0.937	−2.715	0.918	−0.880	0.861	−2.061	0.741
3	−4.208	0.928	−3.802	0.938	−2.997	0.825	−3.110	0.818
4	−4.779	0.937	−4.704	0.947	−4.258	0.866	−4.246	0.880
5	−5.747	0.970	−5.746	0.970	−6.018	0.775	−6.027	0.921
6	−7.149	0.990	−7.149	0.990	−8.313	0.950	−8.313	0.950
7	−8.918	0.999	−8.918	0.999	−11.226	0.922	−11.227	0.956

Table A.2 — continued

Level	$(\varepsilon_2, \varepsilon_4, \gamma) = (0.235, 0.017, 0°)$				$(\varepsilon_2, \varepsilon_4, \gamma) = (0.389, 0.033, 18°)$			
	$\alpha = 1/2$		$\alpha = -1/2$		$\alpha = 1/2$		$\alpha = -1/2$	
	e_i	a^2	e_i	a^2	e_i	a^2	e_i	a^2
$6i_{11/2}$; 1	−6.463	0.880	−7.182	0.874	−4.371	0.783	−5.726	0.477○
2	−7.857	0.880	−8.412	0.872	−6.915	0.599	−6.736	0.702
3	−8.945	0.839	−9.093	0.855	−8.198	0.579	−8.192	0.751
$7i_{15/2}$; 1					−3.591	0.857	−5.124	0.477
2					−6.496	0.583	−7.116	0.844
3					−7.829	0.813	−7.511	0.826
4					−8.599	0.850	−8.665	0.828

○: Label corresponds to largest component but $a^2 < 0.5$.
●: Label does not correspond to largest component.

used also for the quasiparticle levels. Due to the double dimension of the quasiparticle space, each single-particle level gives rise to two quasiparticle levels of opposite signature, one above and one below the Fermi surface. Observing that the proton number is 71, the relation between the labeling of the quasiparticle levels in Fig. 7 and the single-particle levels in Fig. 9 is easily understood.

Often quasiparticle levels are assigned ordering numbers by counting their position relative to the Fermi surface (see e.g. Ref. [13]). This is, however, not appropriate, since levels will cross the Fermi surface as the deformation changes. Therefore, a given label, assigned in this way, will not necessarily refer to the same diabatic level at different deformation grid points, which complicates the construction of diabatic energy surfaces.

To the extent that diabatic quasiparticle levels can be constructed as a function of the rotational frequency, the labels can straightforwardly be assigned to the levels also at higher rotational frequencies. The presently used method [12,14] for constructing diabatic quasiparticle levels does not work fully satisfactory, but improved techniques are being developed [3]. To give an illustration of what can be expected we show in Table A.2 the squared amplitudes for the label component of the wave function for all quasiparticle levels within a distance of about 10 MeV from the Fermi surface for the deformations ($\varepsilon_2 = 0.235$, $\varepsilon_4 = 0.017$, $\gamma = 0°$) and ($\varepsilon_2 = 0.389$, $\varepsilon_4 = 0.033$, $\gamma = 18°$) at the rotational frequency $\hbar\omega = 0.25$ MeV. For most of the levels, the label corresponds to the largest component of the wave function. Low values for the squared amplitudes of the label components are in a few cases partly due to problems in constructing diabatic levels with the presently used method [12,14].

A.4. Definition of subshell occupation numbers

With the labels $N\ell j; \nu$, where ν is the ordering number, assigned to the quasiparticle levels, a given diabatic level can easily be identified at different deformations and its

occupation number calculated. This leads to an important simplification for a qualitative discussion of structural differences between different nuclear shapes. For example, the total occupation of the diabatic levels originating from a given subshell and thus having the same N, ℓ and j can easily be calculated. For a fully occupied subshell this number is $2j + 1$. Differences in the subshell occupation have been used when comparing the structure of shape coexisting states in ^{165}Lu, as illustrated in Fig. 10.

References

[1] W. Nazarewicz, M.A. Riley and J.D. Garrett, Nucl. Phys. A 512 (1990) 61.
[2] D. Müller, A. Virtanen, R. Julin, S. Juutinen, A. Lampinen, S. Törmänen, F. Christancho, A.P. Byrne, G.D. Dracoulis, B. Fabricius, C. Fahlander, A. Johnson, K.P. Lieb, J. Nyberg, I. Thorslund and R. Wyss, Phys. Lett. B 332 (1994) 265.
[3] R.A. Bark, R. Bengtsson and H. Carlsson, Phys. Lett. B 339 (1994) 11.
[4] W. Schmitz, C.X. Yang, H. Hübel, A.P. Burne, R. Musseler, N. Singh, K.H. Maier, A. Kuhnert and R. Wyss, Nucl. Phys. A 539 (1992) 112.
[5] W. Schmitz, H. Hubel, C.X. Yang, G. Baldsiefen, G. Frölingsdorf, D. Metha,R. Musseler, M. Neffgen, P. Willsau, J. Gascon, G.B. Hagemann, A. Maj, D. Müller, J. Nyberg, M. Piiparinen, A. Virtanen and R. Wyss, Phys. Lett. B 303 (1993) 230.
[6] R. Wyss, private communication (1993).
[7] B. Herskind, Nucl. Phys. A 447 (1986) 395c.
[8] G. Sletten, J. Gascon and J. Nyberg, Proc. Int. Conf. on the Spectroscopy of Heavy Nuclei, Crete, June 1989, eds. J.F. Sharpey-Shafer and L.D. Skouras, Inst. of Phys. Conf. Series No. 105 (Inst. of Phys., Bristol, 1989) p. 125.
[9] D.C. Radford, Nucl. Inst. Meth., to be published.
[10] S. Jónsson, J. Lyttkens, L. Carlen, N. Roy, H. Ryde, W. Walus, J. Kownacki, G.B. Hagemann, B. Herskind and J.D. Garrett, Nucl. Phys. A 422 (1984) 397.
[11] P. Frandsen, R. Chapman, J.D. Garrett, G.B. Hagemann, B. Herskind, C.-H. Yu, K. Schiffer, D. Clarke, F. Khazaie, J.C. Lisle, J.N. Mo, L. Carlen, P. Ekström and H. Ryde, Nucl. Phys. A 489 (1988) 508.
[12] T. Bengtsson, Nucl. Phys. A 496 (1989) 56; A 512 (1990) 124.
[13] R. Bengtsson, T. Bengtsson, M. Bergström, H. Ryde and G.B. Hagemann, Nucl. Phys. A 569 (1994) 469.
[14] T. Bengtsson, Understanding the Ultimate Cranker, Lund Institute of Technology, Department of Mathematical Physics report.
[15] T. Bengtsson and I. Ragnarsson, Nucl. Phys. A 436 (1985) 14.
[16] I. Ragnarsson, Phys. Rev. Lett. 62 (1989) 2084.
[17] A. Brockstedt, J. Lyttkens-Lindén, M. Bergström, L.P. Ekström, H. Ryde, J.C. Bacelar, J.D. Garrett, G.B. Hagemann, B. Herskind, F.R. May, P.O. Tjøm and S. Frauendorf, Nucl. Phys. A 571 (1994) 337.
[18] R. Bengtsson, Nucl. Phys. A 557 (1993) 277c.
[19] H. Frisk and R. Bengtsson, Phys. Lett. B 196 (1987) 14.
[20] R. Bengtsson, Nucl. Phys. A 520 (1990) 201c.
[21] R.A. Bark, G.D. Dracoulis, A.E. Stuchbery, A.P. Byrne, A.M. Baxter, F. Riess and P.K. Weng, Nucl. Phys. A 501 (1989) 157.
[22] R. Bengtsson, J. Dudek, W. Nazarewicz and P. Olanders, Phys. Scrip. 39 (1989) 196.
[23] S.G. Nilsson, C.F. Tsang, A. Sobiczewski, Z. Szymański, S. Wycech, C. Gustafsson, I.-L. Lamm, P. Möller and B. Nilsson, Nucl. Phys. A 131 (1969) 1.